LBNL-41273
UC-413

ERNEST ORLANDO LAWRENCE BERKELEY NATIONAL LABORATORY

Phase Transitions in Nuclear Physics

L.G. Moretto, L. Phair, and G.J. Wozniak

Nuclear Science Division

August 1997

Presented at the
Fifth International Workshop on Relativistic Aspects of Nuclear Physics,
Rio de Janeiro, Brazil,
August 27–29, 1997,
and to be published in
the Proceedings

REFERENCE COPY
Does Not
Circulate

Bldg. 50 Library - Ref.
Lawrence Berkeley National Laboratory

LBNL-41273
Copy 1

DISCLAIMER

This document was prepared as an account of work sponsored by the United States Government. While this document is believed to contain correct information, neither the United States Government nor any agency thereof, nor the Regents of the University of California, nor any of their employees, makes any warranty, express or implied, or assumes any legal responsibility for the accuracy, completeness, or usefulness of any information, apparatus, product, or process disclosed, or represents that its use would not infringe privately owned rights. Reference herein to any specific commercial product, process, or service by its trade name, trademark, manufacturer, or otherwise, does not necessarily constitute or imply its endorsement, recommendation, or favoring by the United States Government or any agency thereof, or the Regents of the University of California. The views and opinions of authors expressed herein do not necessarily state or reflect those of the United States Government or any agency thereof or the Regents of the University of California.

LBNL-41273
UC-413

Phase Transitions in Nuclear Physics

L.G. Moretto, L. Phair and G. J. Wozniak

Nuclear Science Division
Ernest Orlando Lawrence Berkeley National Laboratory
University of California, Berkeley, California 94720 USA

August 1997

This work was supported in part by the Director, Office of Energy Research, Office of High Energy and Nuclear Physics, Division of High Energy Physics, of the U.S. Department of Energy under Contract No. DE-AC03-76SF00098.

Phase Transitions in Nuclear Physics

L.G. Moretto L. Phair, and G.J. Wozniak

Nuclear Science Division, Lawrence Berkeley National Laboratory,
1 Cyclotron Rd, Berkeley, CA 94720, USA

Abstract

A critical overview of the low energy phase transitions in nuclei is presented with particular attention to the 2nd (1st) order pairing phase transitions, and to the 1st order liquid-vapor phase transition. The role of fluctuations in washing out these transitions is discussed and illustrated with examples. A robust indicator of phase coexistence in multifragmentation is presented.

1 Introduction

The application of statistical mechanics to nuclear systems, and the introduction of thermodynamical concepts and jargon in nuclear physics can be traced back to the origin of the field. While the use of statistical mechanics has been very useful in many areas, the associated use of the thermodynamic limit ($N \rightarrow \infty$), on the one hand, has permitted the manipulation of familiar quantities, like temperature, entropy, free energy, etc.; on the other hand, its use has frequently led to the reckless disregard of fluctuations and of their essential role in a small system like a nucleus.

Nowhere has this problem created more confusion than in the discussion of phase transitions. The recent messianic promises of the quark-gluon plasma phase transition may be wisely considered in the light of the "other" phase transitions that have been predicted and looked for in nuclei throughout the history of nuclear physics. In this presentation, we shall examine several features that have been described either theoretically, or in a handwaving manner, as associated with phase transitions. It will not escape even the most casual peruser that almost no experimental data accompany this presentation. The reason for this will hopefully become clear as we proceed with our discussion.

Here is the list of the alleged phase transitions:

1) The "melting" of shell effects with increasing temperature.

2) The 1st (2nd) order phase transition associated with nuclear deformation.

3) The 2nd order phase transition associated with the disappearance of pairing with increasing temperature and/or angular momentum.

4) The 1st order phase transition associated with the disappearance of pairing with increasing quasi particle number.

5) The 1st (2nd) order liquid-vapor phase transition.

Before embarking on a detailed description of these five cases, we are going to review some general features associated with 1st and 2nd order phase transitions, with particular attention paid to fluctuations and their role as spoilers in the characterization of both phases, and phase transitions.

2 General considerations of phase transitions

Let us begin by defining the order of a phase transition. A phase transition is said to be 1st, 2nd, 3rd, etc. order if a singularity is found in the 1st, 2nd, 3rd, etc. derivative with respect to temperature T of the enthalpy H at constant pressure, or of the energy E at constant volume. Therefore, in a 1st order transition, the specific heat c_p or c_v has a singularity, while in a 2nd order transition the specific heat has only a discontinuity, etc.

2.1 Triviality of 1st order phase transitions

The great attention to the alleged discovery of a 1st order liquid-vapor phase transition in nuclear multifragmentation [1] may suggest that this phenomenon could be of great significance to our understanding of nuclear systems. Nothing is farther from the truth. In fact, it is easy to show that 1st order phase transitions are completely trivial [2]. Here are the reasons:

1) If there are two or more distinct phases known, or even hypothetically describable, then there must be a 1st order phase transition.

2) The thermodynamics of the 1st order transition is *completely* determined by the thermodynamical properties of each individual isolated phase. These phases do not affect each other, and do not need to be in contact.

As an example, let us consider Fig. 1, where the molar free energy F at constant T is plotted versus the molar volume for the liquid and gas phases. Stability of each phase requires that each of these curves be concave. The very existence of these

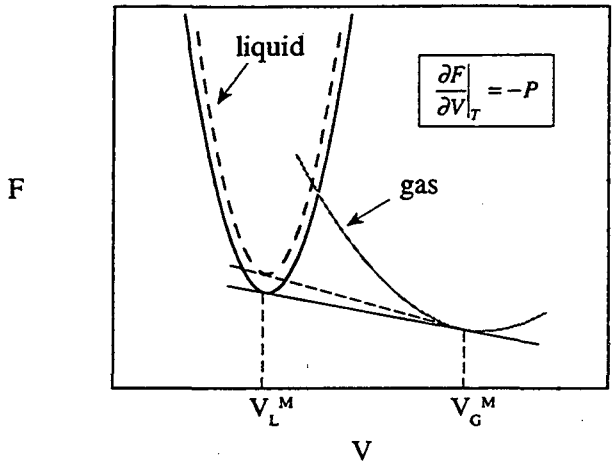

Fig. 1. The free energy as a function of molar volume for a liquid and gas. The dashed lines refer to a drop rather than to bulk liquid.

two concave curves implies that in the region between the points of contact of the common tangent, the free energy is minimized by apportioning the system between the liquid and gas phases. Each phase is defined at the point of tangency, and the segment of the tangent between the two points is the actual free energy of the mixed phase. The slope of the common tangent is the negative of the constant pressure at which the transition takes place. The coexistence region is completely defined by the properties of the liquid at V_L^M and and of the gas at V_G^M. Furthermore, since the liquid is highly incompressible, the point of tangency is near the absolute minimum of F_L. Consequently, it is irrelevant whether the liquid is in contact with the vapor or not!

This discussion applies to infinite phases. However, it is simple to introduce finite size effects, e.g. surface effects.

The Clapeyron equation is:

$$\frac{dP}{dT} = \frac{\Delta H_m}{T \Delta V_m} \tag{1}$$

where P is the vapor pressure, T is the temperature, ΔH_m is the molar enthalpy of vaporization, and ΔV_m is the corresponding change in molar volume. We can write:

$$\Delta H_m = \Delta H_m^0 - c_s S_m = \Delta H_m^0 - 3\frac{c_s V_m}{r} \tag{2}$$

where c_s is the surface energy coefficient, S_m is the molar surface of the drop of liquid, V_m is the molar volume, and r is the radius of the droplet.

Integrating the Clapeyron equation we obtain:

$$P = P_0 \exp\left[-\frac{\Delta H_m}{T}\right] = P_{\text{inf}} \exp\left[\frac{3c_s V_m}{rT}\right] \tag{3}$$

where P_{inf} is the vapor pressure of the infinite liquid. Since the vapor pressure of a drop is always greater than that of the infinite liquid, the common tangent (dashed line, Fig. 1) becomes steeper, in accordance with the increased free energy of the liquid.

2.2 Microcanonical or Canonical Ensemble?

Any good textbook of statistical mechanics contains the demonstration that, in the thermodynamic limit, all ensembles are equivalent, i.e. they give the same thermodynamic functions.

In dealing with phase transitions in finite systems, one may question whether this equivalence is retained. Let us review the connection between, for instance, the Microcanonical and the Canonical Ensemble.

Let $\rho(E)$ be the microcanonical level density. The corresponding canonical partition function is its Laplace transform:

$$Z(\beta) = \sum e^{-\beta E_i} \approx \int \rho(E) e^{-\beta E} dE. \tag{4}$$

The partition function is usually easier to calculate than the level density. However, the latter can be obtained from the former through the inverse Laplace transform:

$$\rho(E) = \frac{1}{2\pi i} \oint Z(\beta) e^{\beta E} d\beta. \tag{5}$$

The integral can be evaluated by the saddle point approximation:

$$\rho(E) = \frac{1}{2\pi i} e^{\ln Z_0 + \beta_0 E} \int e^{-\frac{1}{2}\left.\frac{\partial^2 \ln Z}{\partial \beta^2}\right|_{\beta_0} (\beta-\beta_0)^2} i d(\beta - \beta_0) = \frac{\exp\left(\ln Z_0 + \beta_0 E\right)}{\left(2\pi \left.\frac{\partial^2 \ln Z}{\partial \beta^2}\right|_{\beta_0}\right)^{1/2}}. \tag{6}$$

We can write Eq. (6) as:

$$S_{\text{Micro}} = \ln \rho(E) = \ln Z_0 + \beta_0 E - \frac{1}{2} \ln\left(2\pi \left.\frac{\partial^2 \ln Z}{\partial \beta^2}\right|_{\beta_0}\right) \tag{7}$$

where β_0 corresponds to the stationary point of the integrand. Furthermore,

$$S_{\text{Micro}} = S_{\text{Can}} - \ln\left(2\pi \left.\frac{\partial^2 \ln Z}{\partial \beta^2}\right|_{\beta_0}\right). \tag{8}$$

The first term to the right is of order N while the second is of order $\ln N$.

When N goes to infinity (thermodynamic limit), one can disregard the term of order $\ln N$. For finite N one can easily evaluate the correction term which turns out to be very accurate even for small N. For instance, consider a percolation system with N bonds of which n are broken. The microcanonical level density can be calculated directly:

$$\rho = \frac{N!}{n!(N-n)!}. \tag{9}$$

The inverse Laplace transform yields:

$$\rho = \frac{N^N}{(N-n)^{N-n} n^n} \Big/ \left(2\pi \frac{n(N-n)}{N}\right)^{1/2}. \tag{10}$$

As an example of a finite system, let us take N=6 and n=3. The exact expression yields ρ=20. The saddle point approximation yields ρ=20.6. One can see that with little additional effort one can retain the use of the partition function with little loss of accuracy even for the smallest systems!

Still, in the mind of some physicists there is the bias that a microcanonical approach, or its equivalent through the inverse Laplace transform of the partition function, is more correct than the canonical approach because the former conserves energy, while the latter does not.

In fact, the microcanonical distribution is given by:

$$P(E) = \delta\left(E(p,q) - E_0\right). \tag{11}$$

The canonical distribution instead is given by:

$$P(E) = K e^{-\beta E(p,q)}. \tag{12}$$

In this case, there are energy fluctuations.

So, which is ultimately the "right" ensemble? If it does not matter, as in the the thermodynamic limit, the point is moot. But for finite systems it matters. However, consider the case of a small system which is a part of a larger system. Let us call the total energy E and that of the small system ϵ. Then

$$\begin{aligned} S(E,\epsilon) &= S(E,0) + \left.\frac{\partial S}{\partial \epsilon}\right|_{\epsilon=0} \epsilon + \ldots \\ &= S(E,0) - \frac{\epsilon}{T} + \ldots \end{aligned} \tag{13}$$

Thus,

$$\rho(E,\epsilon) \approx \rho(E,0)e^{-\epsilon/T}. \tag{14}$$

The energy of the small system is canonically distributed, in a real, physical sense. *The canonical, or grand canonical distributions very frequently have a direct physical reality and are not an approximation to a "more correct" microcanonical distribution.* For instance, Na clusters in thermal equilibrium with a carrier gas are canonically distributed in energy.

What is the relevance of the above to phase transitions? There are claims that a microcanonical approach yields "sharper" phase transitions than a canonical approach, because of its lack of energy fluctuations. However, any thermodynamic property, including phase transitions, is defined in statistical mechanics as an ensemble average. *Thus the resulting properties are not properties of the system alone, but they are properties of the ensemble.* So with reference to phase transitions in particular, arguments like "the Microcanonical Ensemble yields sharper phase transitions compared to the Canonical Ensemble, and because of that it is better" are meaningless. If the *physical* ensemble is canonical, the canonical description is the correct one, irrespective of whether it is sharper or fuzzier than the microcanonical description.

2.3 Sharpness of phases and phase transitions

Let us consider the free energy of the liquid phase in Fig. 1. We can expand about the minimum as follows:

$$F = F_0 + \frac{1}{2}\left.\frac{\partial^2 F}{\partial V^2}\right|_{\widehat{V}} (\Delta V)^2. \tag{15}$$

The probability of volume fluctuations are then:

$$P(V) \propto \exp\left[-\frac{(\Delta V)^2}{2\sigma_V^2}\right] \tag{16}$$

where $T/\sigma_V^2 = \partial^2 F/\partial V^2|_{\widehat{V}}$. Since $F \propto N$, $\sigma_V^2 \propto 1/N$. Therefore important volume (density) fluctuations are to be expected at small N. A cluster, or a nucleus, which is not kept artificially at constant density, is going to fluctuate substantially in density.

At coexistence, the correlated fluctuations between the two phases make the sharpness of the phases and of the phase transition even more washed out.

3 Shell Effects and their Disappearance with Excitation Energy

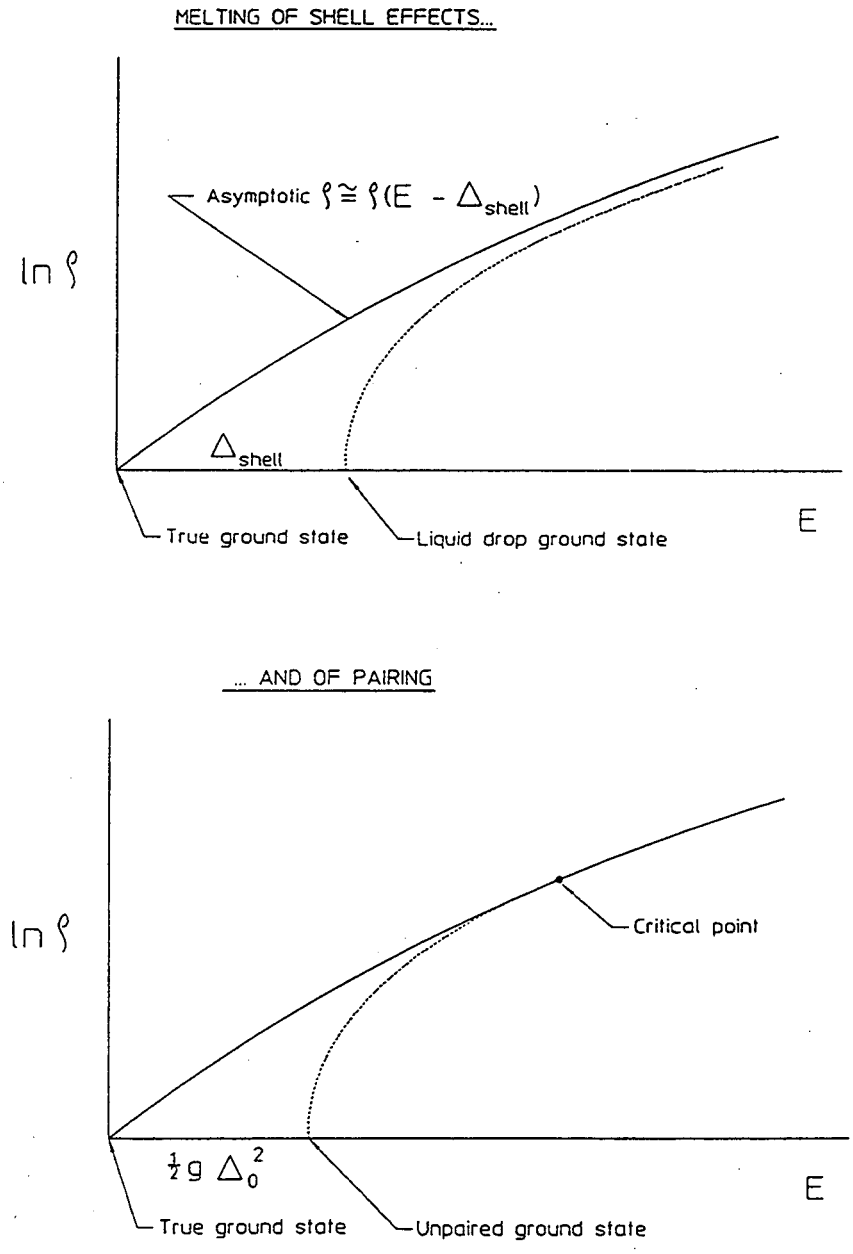

Fig. 2. Schematic presentation of the log of the level density (entropy) as a function of excitation energy demonstrating the effect of shell effects (top panel) and pairing (bottom panel).

Ground state nuclear masses are known to follow a smooth trend with A and Z, as described by the liquid drop model. Superimposed upon this smooth trend there are more or less sharp modulations associated with the magic numbers. Extra stability is observed when the Fermi surface encounters a shell, or even better, a double shell, while diminished stability is observed at mid-shell. The magnitude of the shell effect is clearly due to the sharpness of the Fermi surface and to the gaps in the single particle spectrum. An increase in temperature smears the Fermi surface, and consequently averages the single particle spectrum about the Fermi surface over an energy range proportional to the temperature T, with a corresponding attenuation of the shell

effect [3,4]. This has been occasionally and most improperly called the "melting" of shell effects. This impropriety stems from the fact that this washing out occurs very smoothly. This can be seen in the top panel of Fig. 2, where the logarithm of the level density (the entropy) is plotted vs the excitation energy. For a "Fermi gas" without shell effects, we expect

$$\log \rho \approx S = 2\sqrt{aE}. \tag{17}$$

This square root dependence in a system with a shell effect is reached only asymptotically. Then the expected dependence is achieved provided that the actual excitation energy is corrected for the shell effect

$$\log \rho \approx S = 2\sqrt{a(E-\Delta)}. \tag{18}$$

Thus, there are no steps (1st order), kinks (2nd order) or any other kind of anomalies in the entropy which might justify the use of the expression "phase transition."

4 Phase Transitions in Nuclear Deformation

When the liquid drop nuclear potential energy is plotted versus the deformation parameter ϵ, a broad minimum is observed at sphericity. Shell effects modulate this smooth potential energy, so that additional minima (and maxima) can be observed. For typical deformed nuclei, the deepest minimum is observed at prolate deformations, while a secondary minimum is observed at oblate deformations. This is shown in Fig. 3. For these nuclei, the level density ρ, or the entropy $S = \log \rho$, can be calculated as a function of deformation for various excitation energies [3]. The quantity $\rho(E, \epsilon)$ is therefore the probability of finding the nucleus at the deformation ϵ, and at a given excitation energy E, and is shown schematically in Fig. 4. In Fig. 5 these probability distributions are shown for ^{172}Yb. They characterize completely the statistical properties of this nucleus in so far as deformation is concerned.

One can, however, use the language of thermodynamics to illustrate how, hidden in these distributions, one can find a sort of 1st order phase transition. Two sharp peaks are observed in the deformation probability distributions corresponding to the two minima in the potential energy. A construction analogous to that used for the free energy can be implemented here as shown schematically in Fig. 4. The tangent common to the two entropy maxima is drawn. For any average deformation comprised between the two tangency points, one can apportion the system between the two deformations at tangency in such away that entropy is maximized. The point on the common tangent corresponding to the average deformation represents the maximum possible entropy. The slope of the resulting overall entropy curve represents the

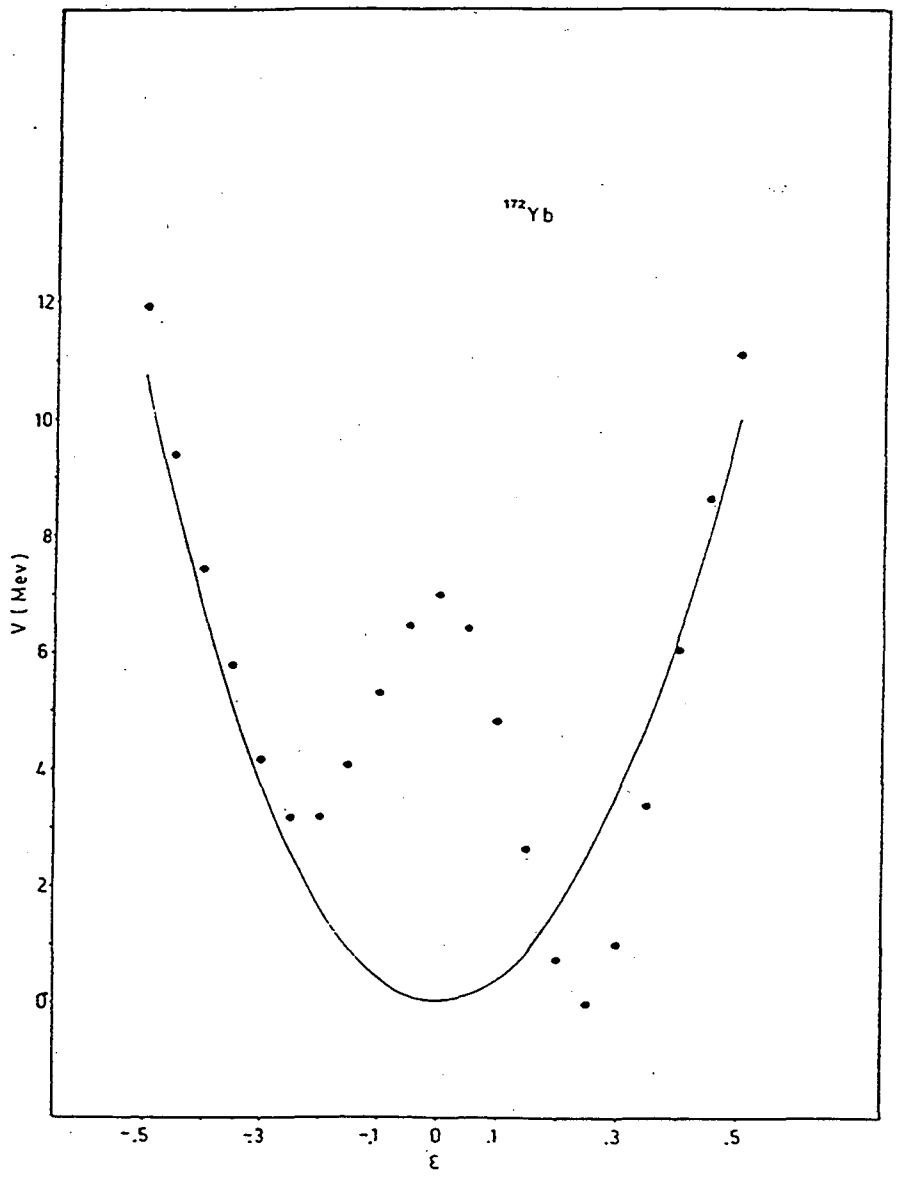

Fig. 3. The calculated potential energy as a function of deformation for ^{172}Yb [3]. The continuous line represents the liquid-drop energy and the solid dots represent the inclusion of shell effects.

"tension" a of the average nucleus

$$\alpha = \left.\frac{\partial S}{\partial \epsilon}\right|_E . \tag{19}$$

At the left of the secondary maximum the tension is highest; along the common tangent branch it remains constant (like the pressure remains constant in a liquid vapor phase transition as a function of average molar volume); it vanishes at the top of the principal maximum; and it turns negative to the right of the maximum. As was pointed out above, this description is completely analogous to that of an ordinary 1st order phase transition. The two entropy peaks correspond to the two distinct nuclear phases, one at oblate and the other at prolate deformations. Unfortunately the "mean deformation" across the transition region is less intuitively helpful than, for instance, the average molar volume, and the "tension" α in the same region is

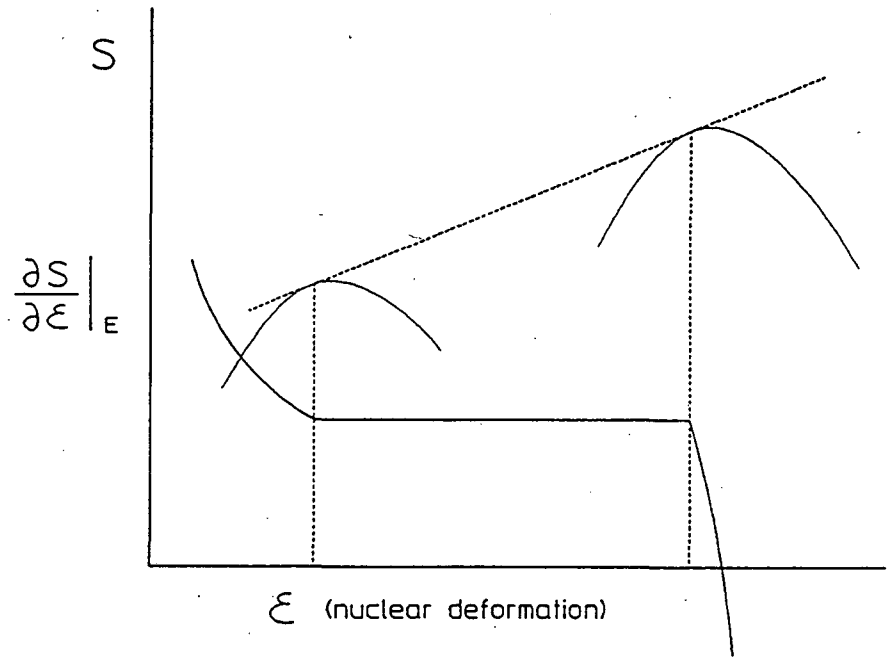

Fig. 4. A schematic presentation of the entropy S (dashed line) and its derivative (solid line) as a function of nuclear deformation.

not quite readily interpretable as the pressure is in a macroscopic phase transition. Of course, to a spectroscopist, such a description may sound meaningless, since, at least at low energy, states can be more or less uniquely assigned to one or the other deformation. On the other hand, this is as close to a macroscopic 1st order phase transition that one has come in nuclear physics.

5 Pairing and the 2nd order Phase Transition

The nuclear Hamiltonian can be written as

$$H = \sum a_k^\dagger a_k \epsilon_k - G \sum a_{k'}^\dagger a_{\bar{k}'}^\dagger a_{\bar{k}} a_k. \tag{20}$$

The first term is the one-body part, and is characterized by the single particle energies ϵ_k; the second term is the two-body part in the pairing approximation, and is characterized by the pairing strength G. The short range attractive nature of the pairing interaction makes this Hamiltonian similar to the BCS Hamiltonian widely applied in superconductivity.

In the Bogoliubov formulation, the auxiliary Hamiltonian H' can be approximately diagonalized in quasi particle space

$$H' = H - \lambda N = \sum (\epsilon_k - \lambda - E_k) + \frac{\Delta^2}{G} + 2\sum n_k E_k, \tag{21}$$

where λ is a Lagrange multiplier to constrain the particle number to the average value N; Δ is the variation parameter (it will become the "order" parameter) or

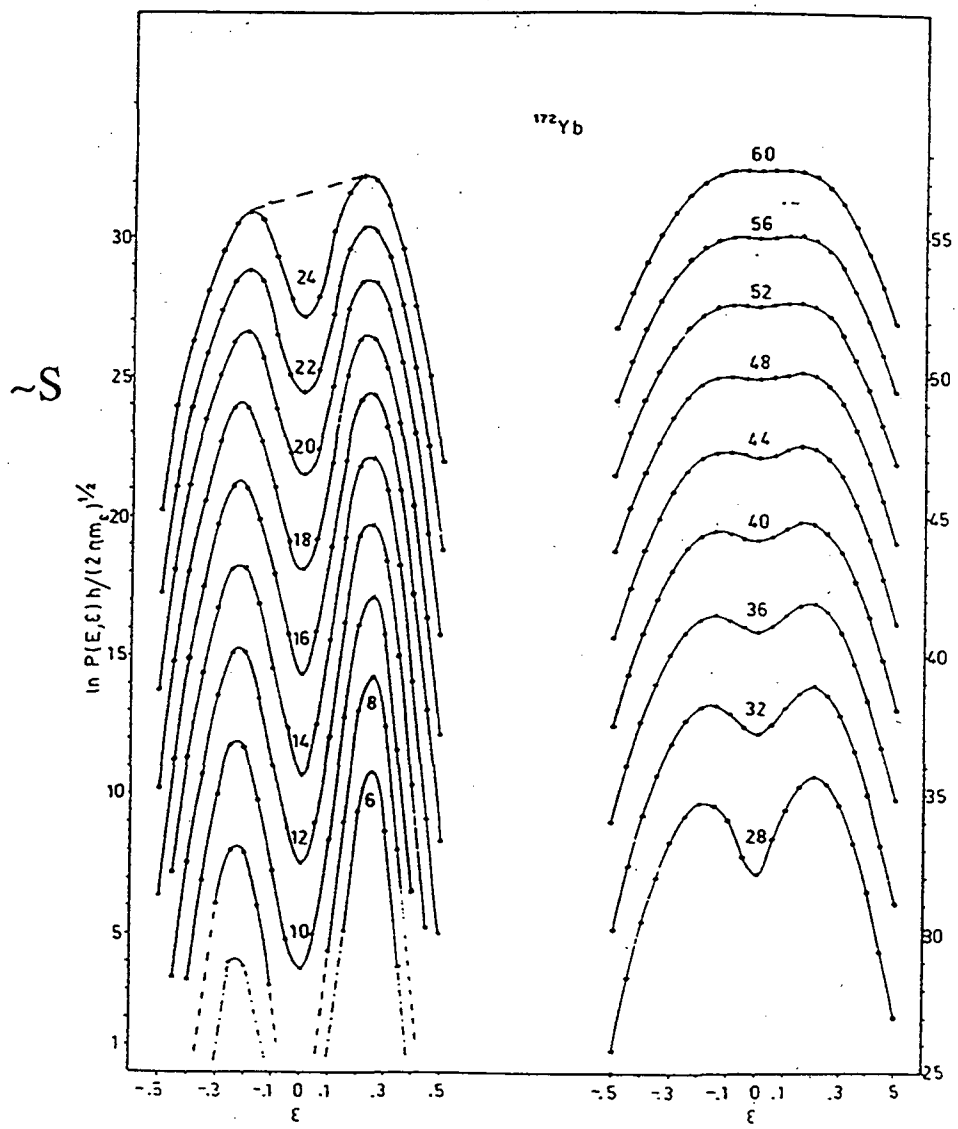

Fig. 5. Natural logarithm of the deformation probabilities for different excitation energies for ^{172}Yb. The labeling of each curve is in MeV.

gap parameter; n_k are the quasi particle occupation numbers; and E_k are the quasi particle excitations given by

$$E_k = \sqrt{(\epsilon_k - \lambda)^2 + \Delta^2}. \tag{22}$$

The gap parameter, in superconductivity is obtained by making the expectation value of H' stationary with respect to Δ:

$$\frac{\partial \langle H' \rangle}{\partial \Delta} = 0. \tag{23}$$

This equation is called the gap equation. It can be solved for Δ for arbitrary occupation numbers of the quasi particle states. If one uses the thermal averages for the occupation numbers, one obtains the temperature dependence of Δ. In the thermal case we can write the Grand Partition Function e^{Ω} as

$$\Omega = -\beta \sum (\epsilon_k - \lambda - E_k) + 2 \sum \log \left(1 + e^{-\beta E_k}\right) - \beta \frac{\Delta}{G} \tag{24}$$

where $\beta = 1/T$. The gap equation is obtained by finding the extremum of Ω with respect to Δ:

$$\frac{\partial \Omega}{\partial \Delta} = 0 \tag{25}$$

or

$$\sum \frac{1}{E_k} \tanh \frac{1}{2} \beta E_k = \frac{2}{G}. \tag{26}$$

The (order) gap parameter decreases with increasing temperature, and goes to zero at a critical temperature with a finite derivative, which results in a discontinuity in the specific heat (2nd order phase transition). Similarly, angular momentum decreases the value of the gap parameter, which goes eventually to zero at a critical value of the angular momentum.

The combined effect of temperature and angular momentum can be seen in Fig. 6 for a realistic case [5]. The line $\Delta(T, I) = 0$ defines the locus of the 2nd order phase transition.

In Fig. 7, again for a realistic case [3], the neutron and proton gap parameters are shown as a function of the excitation energy, together with the specific heat. Notice the big discontinuities of the specific heat corresponding to the neutron and proton 2nd order phase transitions.

6 Pairing and a 1st order phase transition

In the above sections we have allowed the quasi particle number to attain its thermal value without restrictions. Let us now consider what happens when we constrain the quasi particle number to a fixed value Q [6]. In analogy with the above treatment, we introduce the auxiliary Hamiltonian H''

$$H'' = H' - \xi Q \tag{27}$$

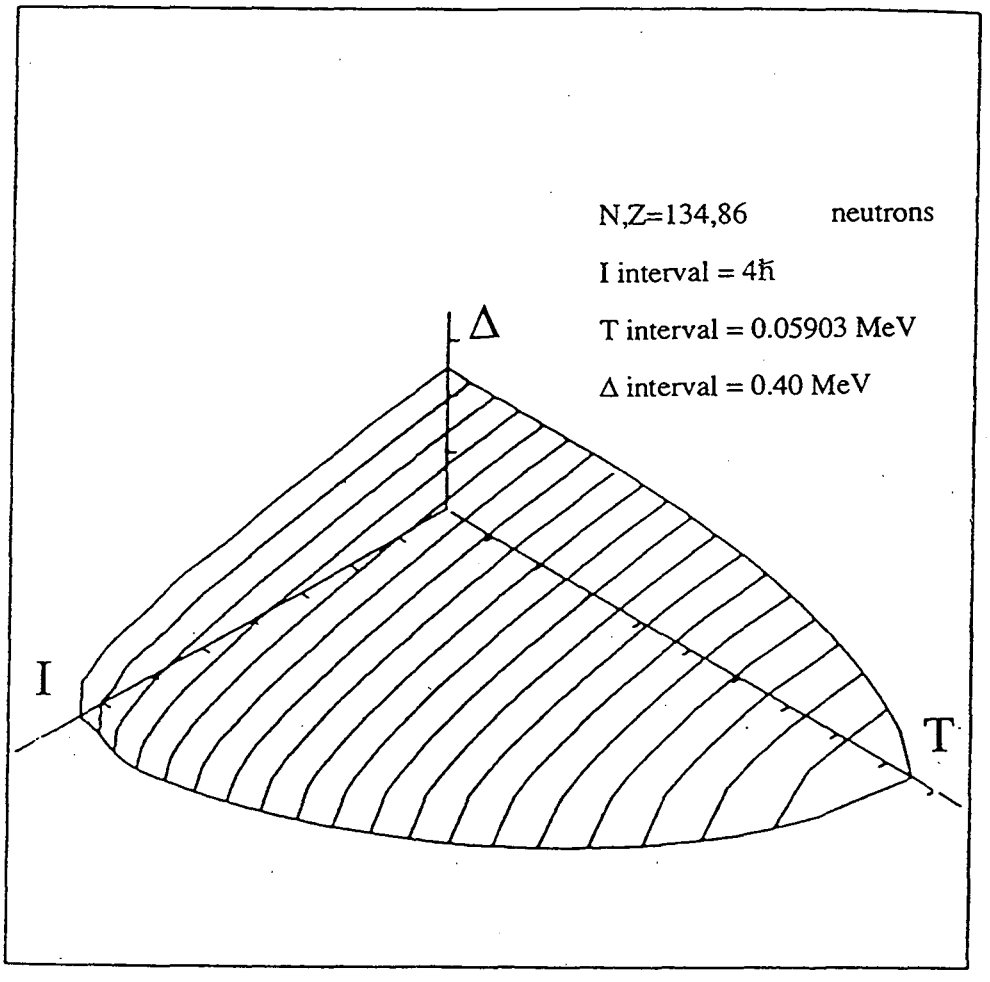

XBL 733-273

Fig. 6. The predicted dependence of Δ on temperature and angular momentum for ^{220}Rn [5].

where $Q = 2\sum n_k$ is the quasi particle and ξ is its Lagrange multiplier. Explicitly

$$H'' = \sum(\epsilon_k - \lambda - E_k) + \frac{\Delta^2}{G} + 2\sum n_k(E_k - \xi)\,. \tag{28}$$

The Grand Partition Function e^{Ω} is readily calculated:

$$\Omega = -\beta\sum(\epsilon_k - \lambda - E_k) + \beta\frac{\Delta^2}{G} + 2\sum\log\left[1 + e^{-\beta(E_k-\xi)}\right]. \tag{29}$$

We now apply this formalism to the uniform model (constant doubly degenerate single particle level density g).

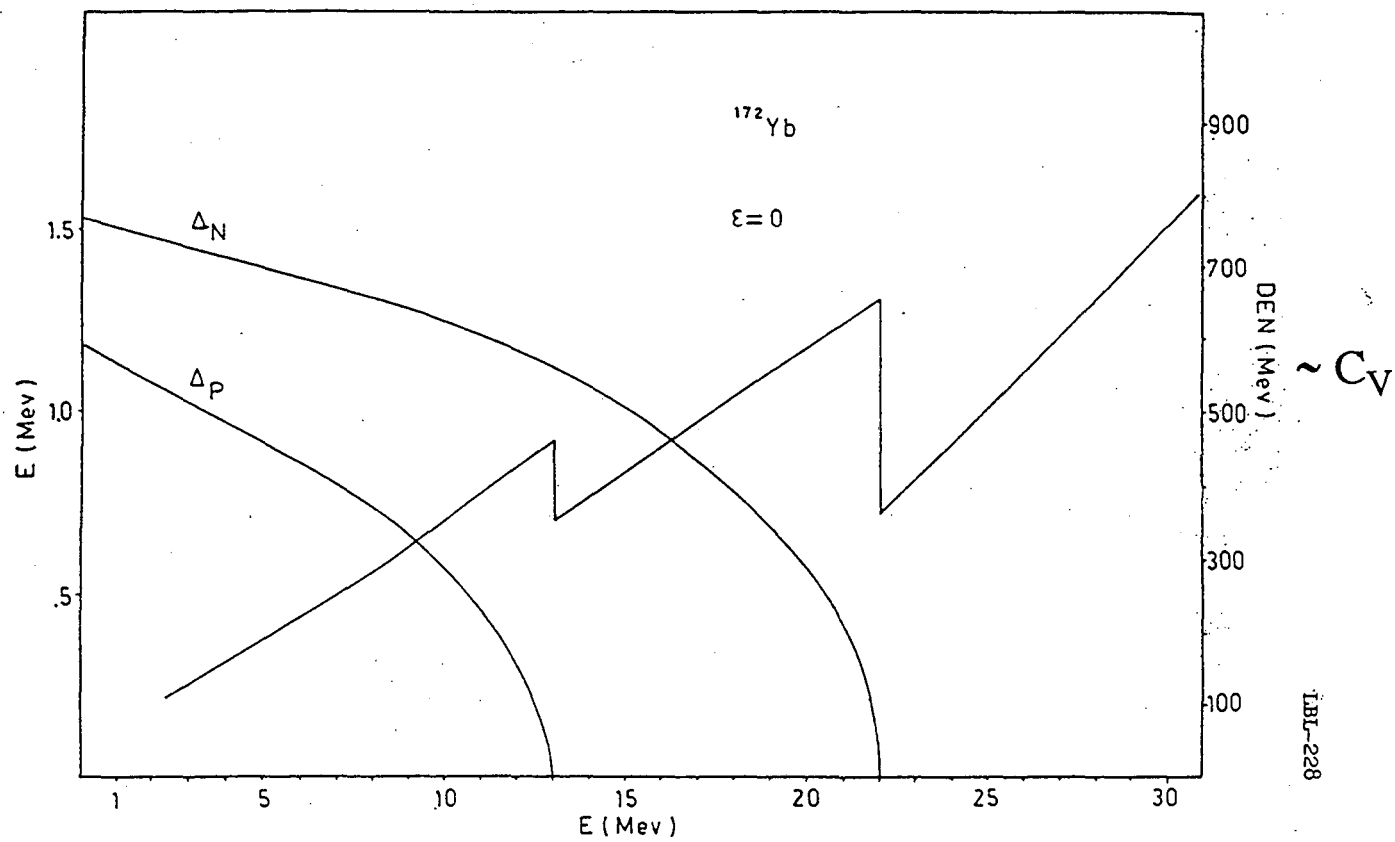

Fig. 7. The calculated neutron and proton gap parameters (left axis) and the specific heat (right axis) as a function of excitation energy for ^{172}Yb at $\epsilon = 0$. The specific heat shows two discontinuities associated with the 2nd order phase transitions.

The limit $T = 0$ can be evaluated analytically; we obtain

$$Q = 2g\sqrt{\frac{\Delta}{\Delta_0}}(\Delta_0 - \Delta) \tag{30}$$

$$E = \frac{1}{2}g\left(\Delta_0^2 - \Delta^2\right)\left(1 + \frac{\Delta}{\Delta_0}\right) \qquad \Delta > 0 \tag{31}$$

$$E = \frac{1}{2}g\Delta_0^2 + \frac{Q^2}{8g} \qquad \Delta = 0 \tag{32}$$

where Δ_0 is the value of the gap parameter Δ at $Q = 0$.

6.1 The Existence of a First-Order Phase Transition

In Fig. 8, the excitation energy is plotted as a function of the quasi-particle number. As the gap parameter Δ goes from Δ_0 to 0, the energy follows a loop. The stable solution is the one with the least energy. Therefore the loop must be bypassed. At

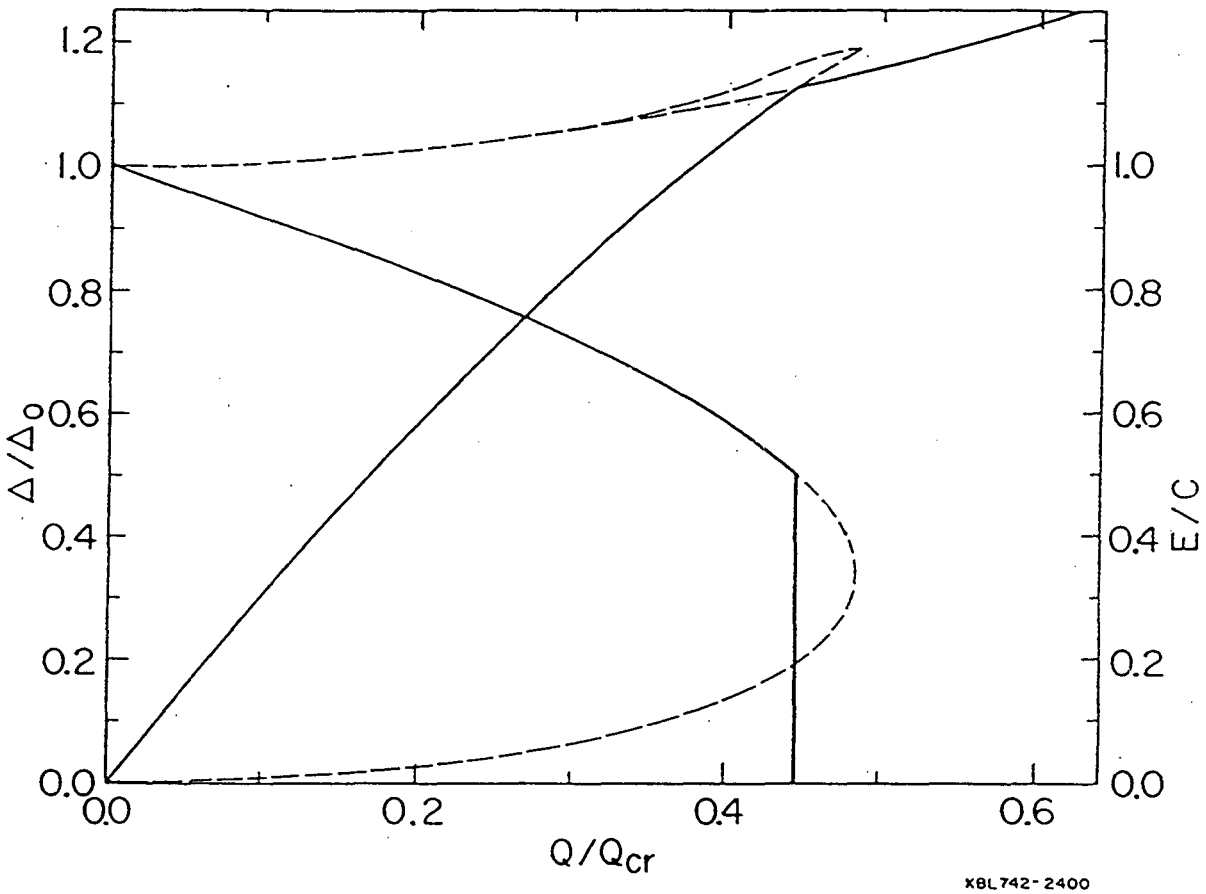

Fig. 8. The gap parameter (left axis) and excitation energy (right axis) are plotted as a function of quasi particle number.

the bypass point the curves for the paired and the unpaired energies cross. Thus the bypass coordinates can be obtained by equating these two energies:

$$E_{\text{paired}} = E_{\text{unpaired}} \tag{33}$$

or

$$\frac{1}{2}g\left(\Delta_0^2 - \Delta^2\right)\left(1 + \frac{\Delta}{\Delta_0}\right) = \frac{1}{2}g\Delta_0^2 + \frac{Q^2}{8g}. \tag{34}$$

This equation together with Eq. (30) gives

$$\frac{\Delta_x}{\Delta_0} = \frac{1}{2} \tag{35}$$

and

$$Q_x = g\frac{\Delta_0}{\sqrt{2}} \tag{36}$$

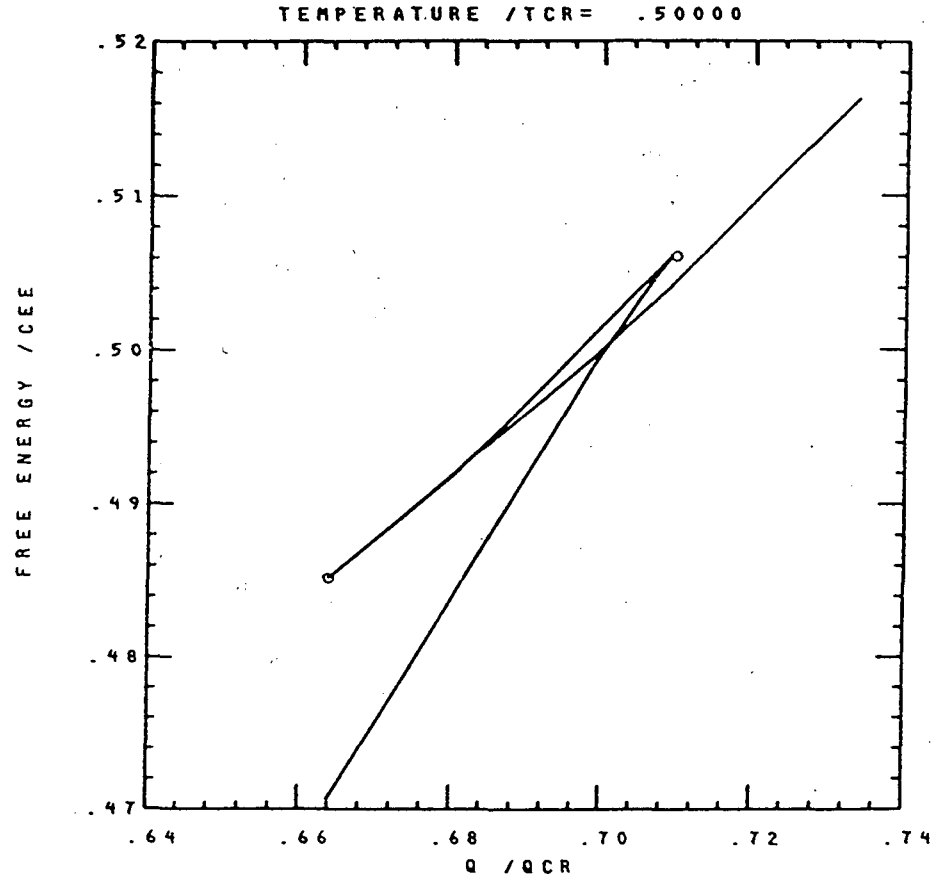

XBL 7411-8556

Fig. 9. The Free Energy is plotted as a function of quasi-particle number for a fixed temperature

where Δ_x and Q_x are the values of Δ and Q at the crossing. The excitation energy at the crossing is:

$$E_x = \frac{9}{8}\left(\frac{1}{2}g\Delta_0^2\right) = \frac{9}{8}C, \tag{37}$$

where C is the pairing condensation energy.

In summary, for values of $Q < Q_x$, the paired solution is the stable one. At $Q = Q_{x'}$, Δ goes abruptly from the value $\Delta_0/2$ to zero and it remains zero for any value of $Q > Q_x$.

This phase transition is much sharper than the one occurring at the critical angular momentum, where Δ goes continuously to zero, but where the first derivative of Δ suffers a discontinuity.

7 Finite Temperature

We now consider the case of finite temperature T.

7.1 Free Energy and Phase Stability

In the region of temperature below T_{cr}, two paired solutions (plus the usual unpaired solutions) appear. In order to determine which of the solutions corresponds to a stable system, the Free Energy F must be investigated. The Free Energy can be obtained from the Grand Partition Function as follows:

$$F = -T\Omega + \xi Q. \tag{38}$$

An example of the dependence of the Free Energy upon Q at a temperature $T < T_{cr}$ is given in Fig. 9. As in the case of $T = 0$, a loop can be observed which must be bypassed by the stable solution. This produces a discontinuous jump from the paired configuration with larger Δ to the unpaired configuration. This isothermal transition is accompanied by an energy change $\Delta E = T\Delta S$, which indicates that indeed one is dealing with a true first-order phase transition.

All of the isotherms present a minimum which corresponds to the equilibrium value of Q if no restriction is set upon the system. Such a minimum satisfies the condition

$$\frac{\partial F}{\partial Q} = \xi = 0. \tag{39}$$

In other words, when the number of quasi-particles is not restricted but is allowed to attain its equilibrium value, the quasi-particle chemical potential is identically zero. Below the critical temperature, the phase transition (first order) occurs for values of Q larger than the equilibrium value. Above the critical temperature, the phase transition (now second order) occurs for values of Q smaller than the equilibrium value.

7.2 The T, Q Diagram and the Plots of Various Thermodynamical Functions

The above information can be used to generate a T, Q diagram. Such a diagram is shown in Fig. 10. The boundary between the paired and the unpaired region defined by the vanishing of the gap parameter Δ is shown. Below the critical temperature such a boundary branches into two lines. The leftmost line corresponds to the continuous vanishing of Δ and it does not correspond to any stable system. The rightmost line corresponds to the discontinuous vanishing of Δ and has physical significance. The solid line characterized by $\xi = 0$, corresponding to the equilibrium number of quasi-particles, is also shown. It starts at the origin of the diagram and stays into the paired region up to the critical temperature, where it exits into the unpaired region. It is along this line that previous pairing calculations have been made.

It is useful now to project various quantities on this basic diagram. In the same figure, the lines of constant energies are projected on the same basic graph. The

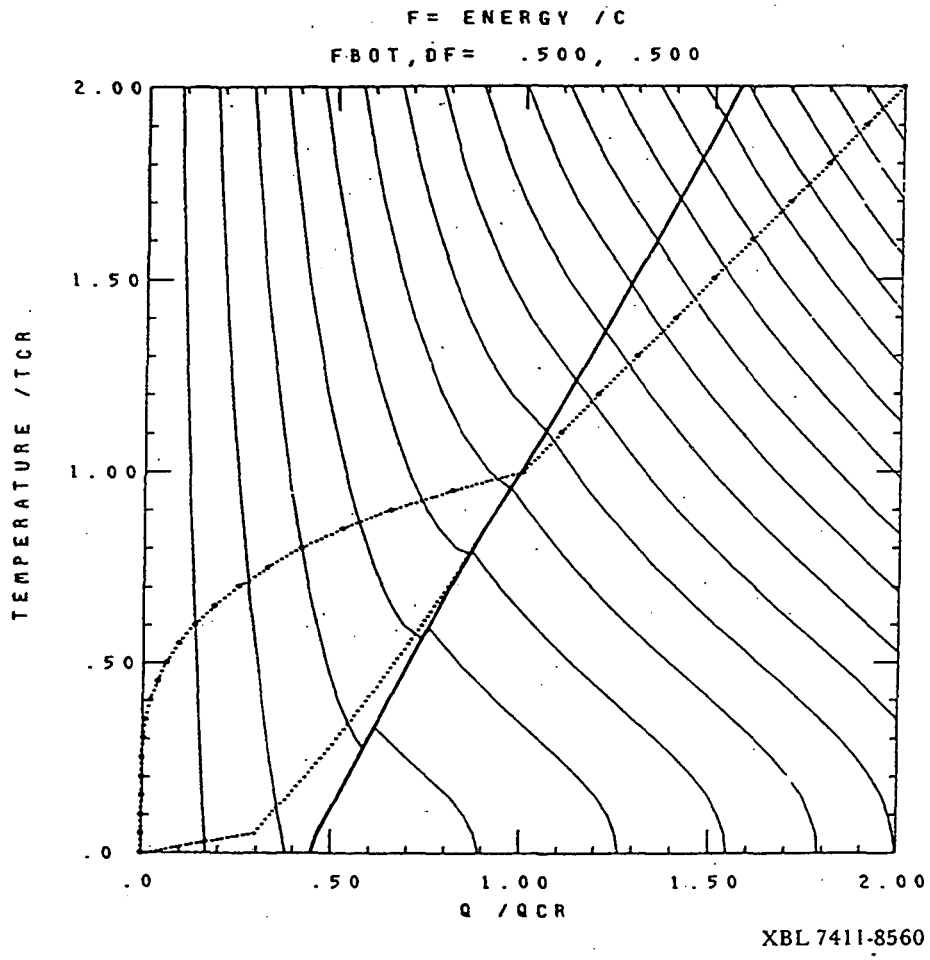

Fig. 10. Lines of constant energy in the T, Q plane. The leftmost line corresponds to $E/C = 0.5$. The lines to the right are spaced in steps of 0.5 E/C. Notice the mismatch of the lines in the region of the first-order phase transition.

temperature, for each line of constant energy, drops dramatically as the quasi-particle number increases. This is due to the larger number of degrees of freedom available to the system with increasing Q. At high temperatures one observes a nearly hyperbolic behavior typical of the Boltzmann limit. The change in the second derivative, visible at low temperature in the paired region, is due to the onset of the strong degeneracy limit.

8 Fluctuations and disappearance of phase transitions

This is all well in the thermodynamical limit. For a small system, however, it is not prudent to take for Δ the value that maximizes Ω at constant T [7]. If we write

$$P(\Delta, T) \propto e^{\Omega(\Delta,T)} \tag{40}$$

we discover that the isothermal distributions of Δ are rather peculiar. In Fig. 11, these distributions are plotted with parameters suitable for a nucleus. At low temperature

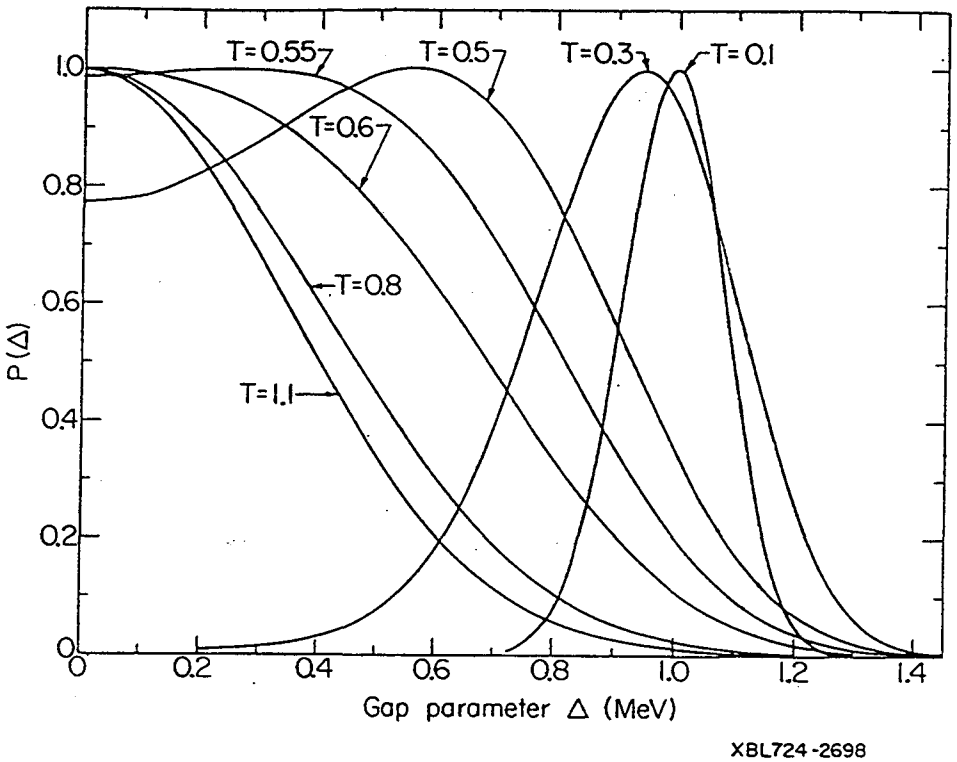

Fig. 11. The distribution of gap parameter values for the indicated temperatures [7]. The critical temperature is at T_{cr}=0.57 MeV.

the distributions are Gaussian-like, and their maximum corresponds to the solution of the gap equation. The width of the distribution is approximately $\sigma^2 = T/g \propto T/N$. Thus, the distribution becomes infinitely narrow in the thermodynamic limit $N \rightarrow \infty$. As the temperature increases, the distributions become broader and skewed, while the peak moves to lower Δ values. At the critical temperature, the peak is located at $\Delta = 0$ but the distribution extends to quite large values of Δ. At temperatures above the critical temperature, the most probable value of Δ remains zero, but the fluctuations are very large. From the figure, it appears that not much happens as we go through the critical temperature. In order to illustrate this, let us consider the quantities averaged over the Δ distribution rather than calculated at the peak. Fig. 12 shows the average value of Δ compared with the most probable value. Clearly the average sails very smoothly through the alleged phase transition. The energy and entropy do not show any kink. Only the specific heat, as illustrated in Fig. 13, shows a broad peak, in lieu of the discontinuity expected in the thermodynamic limit.

9 Phase Transitions, Phase Coexistence, and Charge Distributions

Since the early studies of complex fragment emission at intermediate energies [8–13], a "liquid vapor phase transition" had been claimed as an explanation for the observed power law dependence of the fragment charge distribution. The basis for

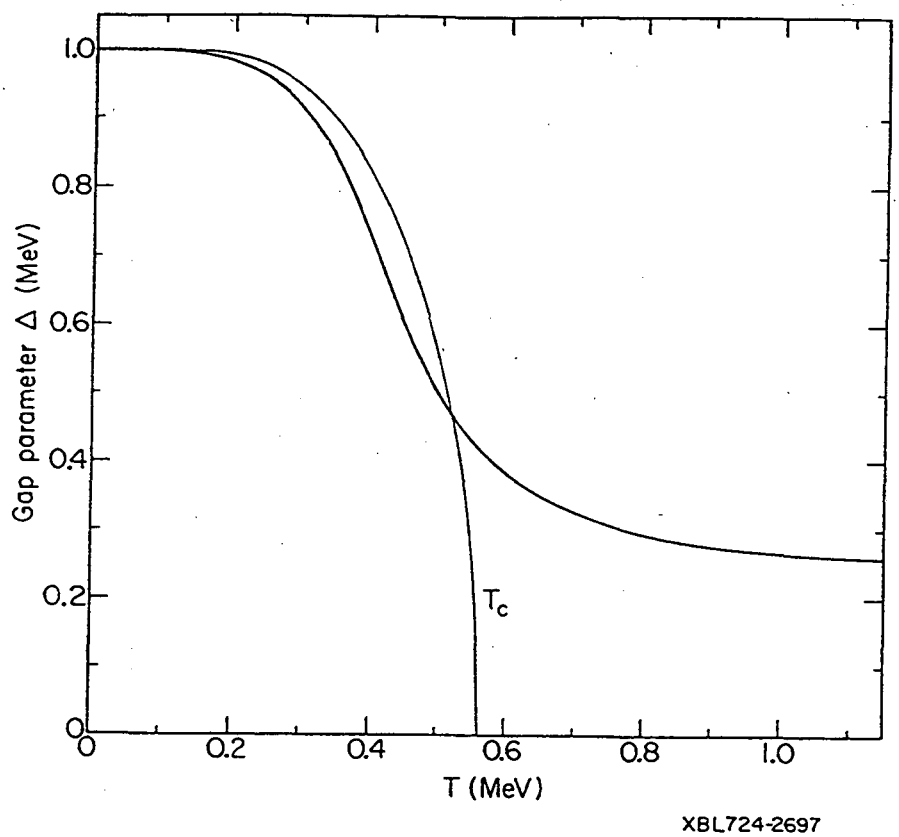

Fig. 12. The average (thick line) and most probable (thin line) value of the gap parameter is plotted as a function of temperature.

such claims was the Fisher droplet theory [14] which was advanced to explain/predict the clusterization of monomers in vapor. According to this theory, the probability of a cluster of size m is given by:

$$P(m) \propto \exp\left[\frac{-(\mu_L - \mu_V)m}{kT}\right] m^{-\tau} \exp\left[-\frac{c_s m^{2/3}}{kT}\right] \tag{41}$$

where μ_L, μ_V are the liquid and vapor chemical potentials, τ is the Fisher critical exponent, and c_s is the surface energy coefficient for the liquid. For $\mu_V > \mu_L$ the liquid phase is stable and large clusters are found. For $\mu_V < \mu_L$ the vapor is stable and small clusters are present. At the critical temperature the liquid-vapor distinction ends, $\mu_L = \mu_V$ and the surface energy coefficient vanishes. The cluster size distribution assumes a characteristic power law dependence.

It was soon realized that power law dependences could be easily generated in more mundane environments. However, a recent analysis of very detailed experiments has claimed not only the demonstration of a near critical regime, but also the determination of other critical coefficients [15] besides τ. Because a detailed description of this analysis would take us far afield, regretfully we must abandon this subject.

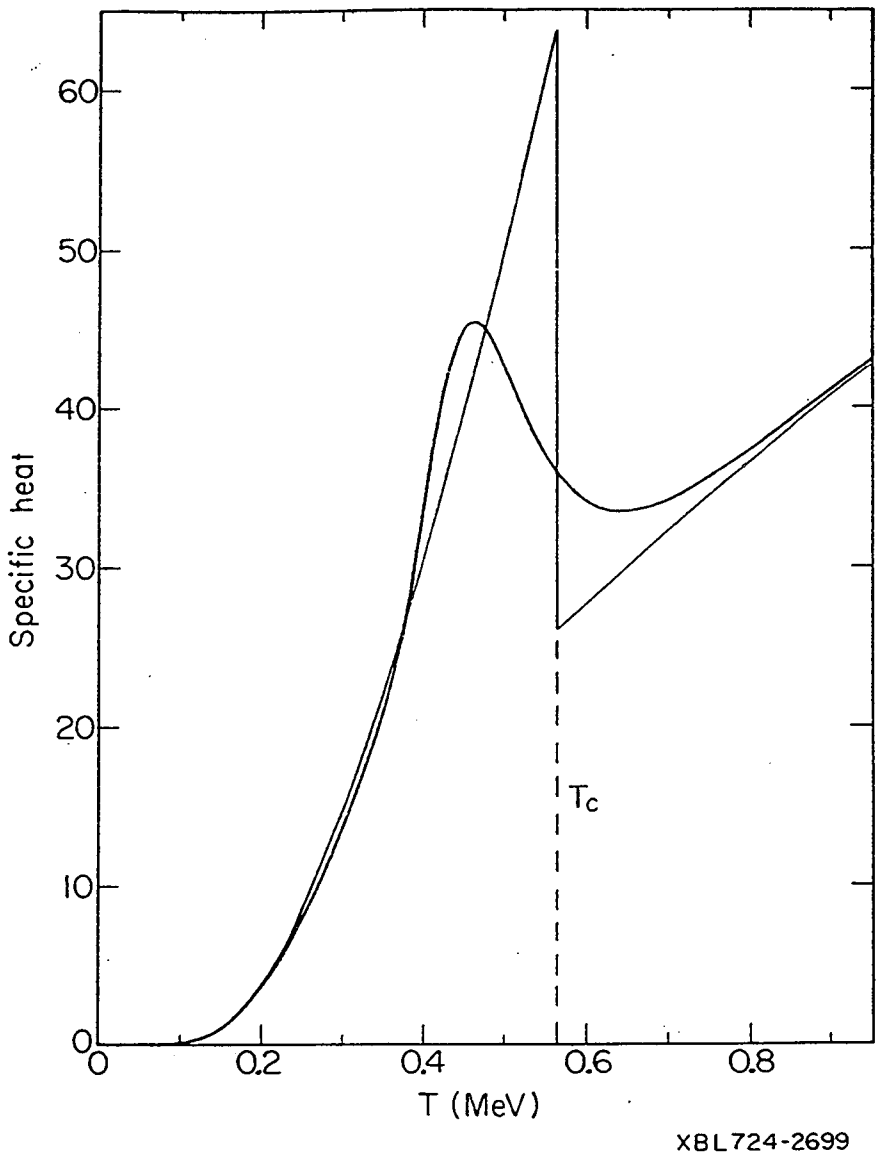

Fig. 13. The average and most probable specific heat is shown as a function of temperature.

However, another recent announcement claiming the discovery of a 1st order phase transition associated with multifragmentation [1] has created a strong resonance. Because of the greater simplicity inherent to this subject, and because of its relevance to some of our work reported below, we discuss it here in some detail.

This study [1] claims to have determined the "caloric curve" (sic) of a nucleus, namely the dependence of nuclear temperature on excitation energy. The temperature is determined from isotopic ratios (e.g. $^3He/^4He$, $^6Li/^7Li$) [16], while the excitation energy is determined through energy balance. Details about these determinations and their possible pitfalls [17–19] will not be discussed here. The highlight of this measurement is the discovery of a plateau, or region of constant temperature, which, in the authors' view, is indicative of a 1st order phase transition from the liquid to the vapor phase.

Apparently, the "paradigm" the authors have in mind is a standard picture of the diagram of temperature T versus enthalpy H for a one component system at *constant pressure* P. In this diagram, the temperature of the liquid (no vapor is present yet!) rises until the vapor pressure p matches the external pressure P. From this point on, the vapor appears and the temperature remains constant until the liquid has completely evaporated. After the liquid has disappeared, the temperature of the (now overheated) vapor can rise again.

It is not clear whether the experimental curve [1] can be interpreted in terms of equilibrium thermodynamics [20]. If this is the case, however, several problems arise. For instance, the claimed distinction between the initial rise (interpreted as the fusion-evaporation regime) and the plateau (hinted at as the liquid-vapor phase transition) is not tenable, since evaporation *is* the liquid-vapor phase transition and no thermodynamic difference exists between evaporation and boiling.

Furthermore, the "caloric curve" requires for its interpretation an additional relationship between the variables T, P, and V. More to the point, the plateau is a very specific feature of the constant pressure condition, rather than being a general indicator of a phase transition. For instance, a constant-volume liquid-vapor phase transition is *not* characterized by a plateau but by a monotonic rise in temperature. This can be easily proven by means of the Clapeyron equation, which gives dP/dT along the univariance line (liquid-vapor transition) together with the ideal-gas equation for the vapor.

For the nearly ideal vapor phase ($P = nT$), we write:

$$dP = Tdn + ndT \tag{42}$$

where n is the vapor molar density. In order to stay on the univariance line, we need the Clapeyron equation:

$$\frac{dP}{dT} = \frac{\Delta H}{T\Delta V} \tag{43}$$

where ΔH is the molar enthalpy of vaporization and ΔV is the molar change in volume from liquid to gas. From this we obtain:

$$n\left(\Delta H - T\right)dT = T^2 dn. \tag{44}$$

At constant pressure, dn=0, so dT=0. For $dn > 0$, we see immediately that $dT > 0$. Using $dE \approx dn\Delta E$, where ΔE is the molar heat of vaporization at constant volume, we finally obtain:

$$\left.\frac{\partial T}{\partial E}\right|_V \approx \frac{T^2}{n\Delta E^2} = \frac{1}{n\Delta S^2}. \tag{45}$$

The positive value of this derivative shows that the phase transition at constant volume is characterized by a monotonic increase in temperature.

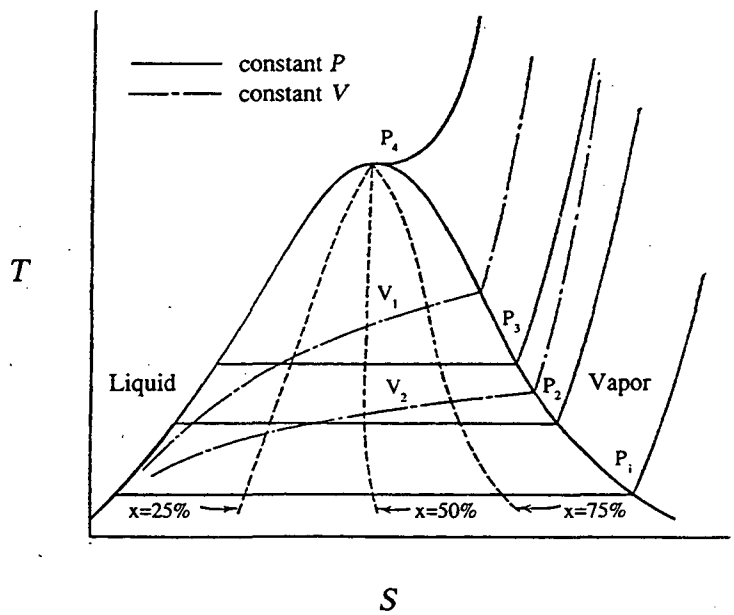

Fig. 14. Temperature-entropy diagram for steam. Curves are shown for constant pressure ($P_4 > P_3 > P_2 > P_1$), constant volume ($V_1 < V_2$) and constant percentage in the gas phase (dashed lines).

As an example, Fig. 14 shows a standard temperature T versus entropy S diagram for water vapor. The region under the bell is the phase coexistence region. For the constant pressure curves ($\Delta S = \Delta H/T$), the initial rise along the "liquid" curve is associated with pure liquid, the plateau with the liquid-vapor phases, and the final rise with overheated vapor. The constant volume curves ($\Delta S = \Delta E/T$), however, cut across the coexistence region at an angle, without evidence for a plateau.

Thus the reminiscence of the observed "caloric curve" with "the paradigm of a phase transition" may be more pictorial than substantive, and indicators other than the plateau may be needed to substantiate a possible transition from one to two phases. More specifically, *an additional relationship* between the three variables P, T, V (like P=const, or V=const, etc.) *is needed to interpret a T-E diagram unequivocally.*

9.1 A robust indicator of phase coexistence

As we have seen, a "generic" caloric curve of the kind obtained in Ref. [1] is of problematic interpretation because of the difficulty in establishing the additional relation

$F(V,T,P)$ associated with the evolution of the system.

Nevertheless, the only meaningful experimental question about 1st order phase transitions is whether the system is present in a single phase, or there is phase coexistence. In thermodynamical language, we want to know whether the system is univariant (two phases), or bivariant (one phase).

We have found a robust indicator for just these features in the charge distributions observed in multifragmentation.

The charge distributions follow a simple scaling [21]:

$$P(Z) \propto \exp\left(-\frac{B}{T} - cnZ\right) \tag{46}$$

where T is the temperature and n is the fragment number. On the other hand, the "charge distribution" arising from the least biased fragmentation into n pieces of an integer Z_0 is [21,22]:

$$P(Z) \approx \frac{n^2}{Z_0} e^{-\frac{nZ}{Z_0}} = cn^2 e^{-cnZ}. \tag{47}$$

While this form obviously implies charge conservation, it is not necessary that charge conservation be implemented as suggested by Eq. (47). In fact it is easy to envisage a regime where the quantity c should be zero. Sequential thermal emission is a case in point. Since each fragment does not know how many other fragments will follow its emission, its charge distribution can not reflect the requirement of an unbiased partition of the total charge among n fragments. Let us consider, for instance, a liquid drop evaporating fragments of different size and binding energy. Charge conservation will affect the distribution minimally, unless evaporation consumes the entire system, and even then, not in the sense of an unbiased partition. A simulation in which fragments with different barriers are allowed to be emitted sequentially according to the binomial scheme of Ref. [23] yields indeed c=0 if a residue survives.

On the other hand, in a simultaneous emission controlled by a n-fragment transition state [24,25], fragments would be strongly aware of each other, and would reflect such an awareness through the charge distribution.

The question then arises whether $c = 0$, or $c > 0$, or even better, whether one can identify a transition from a regime for which $c = 0$ to a new regime for which $c > 0$. To answer this question, we have studied the charge distributions as a function of fragment multiplicity n and transverse energy E_t for a number of systems and excitation energies. Specifically, we will present data for the reaction ^{36}Ar+^{197}Au at E/A=80 and 110 MeV and the reaction ^{129}Xe+^{197}Au at E/A=50 and 60 MeV [22].

Several approaches can be used to extract c from the charge distributions [22]. If the charge distributions are exponential (as is sometimes the case, $P_n(Z) \propto e^{-\alpha_n Z}$),

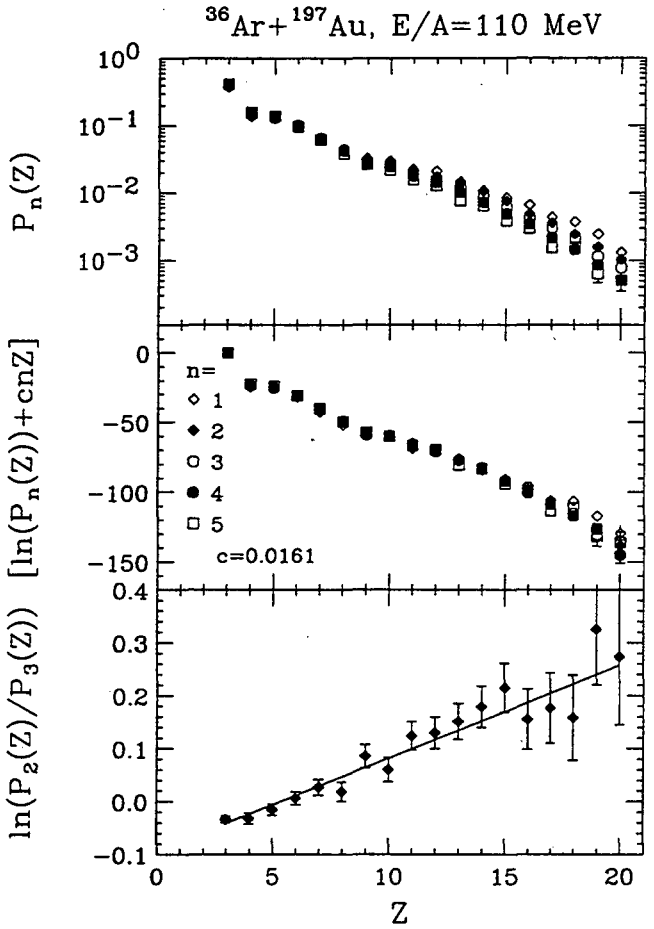

Fig. 15. Top panel: the n gated charge distributions $P_n(Z)$ for the reaction ^{36}Ar+^{197}Au at E/A=110 MeV. The charge distributions were constructed from events with E_t=650±20 MeV and n=1-5. Middle panel: the "reduced" charge distribution [21] for the same data using the indicated value of c. (The data here are normalized at Z=3). Bottom panel: the log of the ratio of $P_2(Z)/P_3(Z)$. The slope corresponds to c for n=2 (see Eq. (48)). The statistical error bars are shown for errors larger than the symbol size.

it is sufficient to extract from them the exponential coefficient α_n [21]. From the n dependence of α_n, the quantity c is readily extracted. A more general approach which does not depend on any specific form for the charge distribution is to construct at each E_t the ratio:

$$\frac{P_n(Z)}{P_{n+1}(Z)} \propto e^{cZ}. \tag{48}$$

A value of c can be extracted for each n by taking the log of this ratio and finding the slope of the resulting graph (see bottom panel of Fig. 15). A weighted average (over all IMF multiplicities n) for c can then be constructed at all E_t. Alternatively, a χ^2 can be constructed in terms of the differences in $P(Z)$ between any pairs of n values and minimized as a function of c [22,26]. These procedures yield essentially the same results which are reported in Fig. 16 for the ^{129}Xe+^{197}Au and ^{36}Ar+^{197}Au reactions.

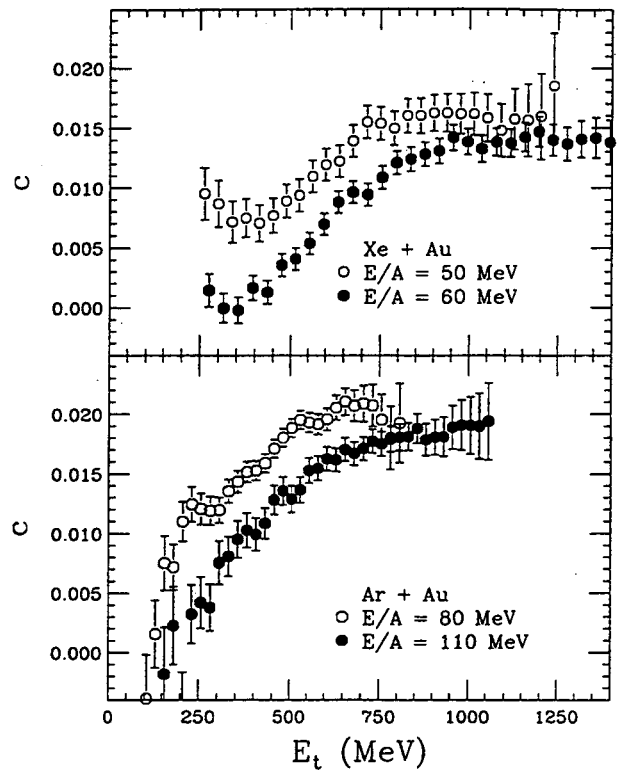

Fig. 16. Plots of the coefficient c versus E_t for the reactions ^{129}Xe+^{197}Au at E/A=50 and 60 MeV (top panel) and ^{36}Ar+^{197}Au at E/A=80 and 110 MeV (bottom panel). The error bars are statistical.

It is interesting to notice that for all reactions and bombarding energies the quantity c starts at or near zero, increases with increasing E_t for small E_t values, and seems to saturate to a constant value at large E_t.

This behavior can be compared to that of a fluid crossing from the region of liquid-vapor coexistence (univariant system) to the region of overheated and unsaturated vapor (bivariant system, see Fig. 17). In the coexistence region, the properties of the saturated vapor cannot depend on the total mass of fluid. The presence of the liquid phase guarantees mass conservation at all average densities for any given temperature. A change in mean density (volume) merely changes the relative amount of the liquid and vapor, without altering the properties of the saturated vapor. Hence the vapor properties, and, in particular, the cluster size distributions cannot reflect the total mass or even the mean density of the system. In our notation, $c = 0$.

On the other hand, in the region of unsaturated vapor, there is no liquid to insure mass conservation. Thus the vapor itself must take care of this conservation, at least grand canonically. In our notation, $c > 0$. In other words we can associate $c = 0$ with thermodynamic univariance, and $c > 0$ with bivariance.

These considerations lead to the immediate identification: $c \propto (\mu_L - \mu_V)$ in the Fischer model [14], where μ_L and μ_V are the chemical potentials of the liquid and the

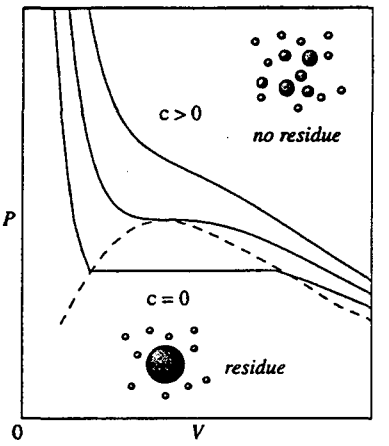

Fig. 17. Liquid-gas phase diagram. The top of the dashed line is the critical point. The area below the dashed line ($c = 0$) is the region where mixtures of the liquid and gas phases coexist.

vapor respectively. Thus, in the coexistence region ($\mu_L = \mu_V$), $c = 0$, while for the overheated vapor ($\mu_V < \mu_L$), $c > 0$.

To test these ideas in finite systems, we have considered a finite percolating system and a system evaporating according to a thermal binomial scheme [23,27]. Percolation calculations [28] were performed for systems of Z_0=97, 160 and 400 as a function of the percentage of bonds broken (p_b). Values of c were extracted (using Eq. (48)) as a function of p_b.

The results are shown in Fig. 18. Guided by the insight gleaned from the approximate solution to Euler's problem (see Eq. (47)) we have scaled the extracted values of c by the source size Z_0 in order to remove this leading dependence and to evidentiate the true finite size effects. For values of p_b smaller than the critical (percolating) value ($p_b^{crit} \approx 0.75$ for an infinite system), we find $c = 0$. This is the region in which a large (percolating) cluster is present. As p_b goes above its critical value, the value of c increases, and eventually saturates in a way similar to that observed experimentally.

Notice that although the phase transition in the infinite system is second order at $p = p_c$, here the region for which $c = 0$ mimics a first order phase transition.

Before proceeding, let us remind ourselves that charge conservation is *not* a finite-size effect. For instance, the chemical potential, introduced in statistical mechanics to conserve mass, survives the thermodynamic limit and retains its meaning for an infinite system, despite the fact that the extensive thermodynamic quantities go to

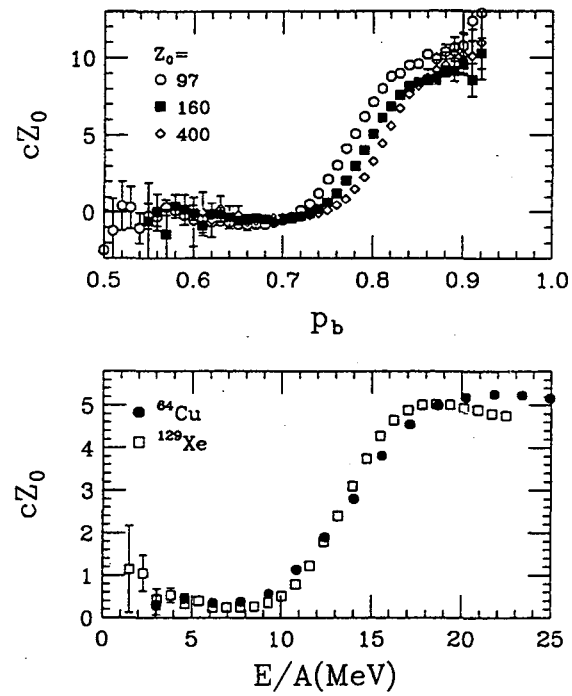

Fig. 18. top: A plot of cZ_0 versus the percentage of broken bonds p_b from a percolation calculation [28] for three systems Z_0=97 (circles), Z_0=160 (squares) and Z_0=400 (diamonds). bottom: A plot of cZ_0 versus excitation energy per nucleon from a binomial evaporation calculation [27] for ^{64}Cu and ^{129}Xe. The statistical error bars are shown for errors larger than the symbol size.

infinity. In our case, while it is true that c goes to zero or that $1/c$ goes to infinity, it is also true that the product cZ_0 tends to a finite limit nearly independent of Z_0.

Our analysis is not directly comparable to the Euler solution (Eq. (47)) since we have restricted ourselves to a limited region ($3 \leq Z \leq 20$) of the total charge distribution for our study of how the source is partitioned into different IMF multiplicities (see ref. [26]). Furthermore, Eq. (47) and the associated dependence of c upon Z_0 are characteristic of a one-dimensional percolation model. Therefore, it is not unexpected that c appears to be proportional, but not equal, to $1/Z_0$ in the three-dimensional percolation calculation reported in Fig. 18.

An evaporation calculation was also carried out for the nuclei ^{64}Cu and ^{129}Xe according to the thermal binomial scheme [23,27]. The only constraint introduced was to prevent at every step the emission of fragments larger than the available source. The extracted quantity cZ_0 is plotted in the bottom panel of Fig. 18 as a function of excitation energy per nucleon. In both cases cZ_0 goes from 0 to a positive finite value (equal for both nuclei) as the energy increases. The region where $c = 0$ is readily identified with the region where a large residue survives. On the other hand, when $c > 0$ there is no surviving residue.

These results are in striking agreement with those obtained for percolation. For both

kinds of finite systems, the univariant regime ($c = 0$) is associated with the presence of a residue, while the bivariant regime ($c > 0$) with the absence of a residue.

This work was supported by the Director, Office of Energy Research, Office of High Energy and Nuclear Physics, Nuclear Physics Division of the US Department of Energy, under contract DE-AC03-76SF00098.

References

[1] J. Pochodzalla *et al.*, Phys. Rev. Lett. **75**, 1040 (1995).

[2] L.G. Moretto, L. Phair, G.J. Wozniak, *Proceedings of CRIS '96 1st Catania Relativistic Ion Studies:* Acicastello, May 27-31, 1996, Costa, Albergo, Insolia, Tuvé eds., World Scientific 1996, p. 46.

[3] L.G. Moretto, Nucl. Phys. A **182**, 641 (1972).

[4] J.R. Huizenga and L.G. Moretto, Ann. Rev. of Nucl. Sci. **22**, 427 1972.

[5] L.G. Moretto, Nucl. Phys. A **185**, 145 (1972); L.G. Moretto, Nucl. Phys. A **216**, 1 (1973).

[6] L.G. Moretto, Phys. Lett. B **51**, 35, (1974); L.G. Moretto, Nucl. Phys. A **243**, 77 (1975).

[7] L.G. Moretto, Phys. Lett. B **40**, 1 (1972); L.G. Moretto, Nucl. Phys. A **226**, 9 (1974).

[8] J.E. Finn *et al.*, Phys. Rev. Lett. **49**, 1321 (1982).

[9] A.D. Panagiotou *et al.*, Phys. Rev. Lett. **52**, 496 (1984).

[10] R.W. Minich *et al.*, Phys. Lett. B **118**, 458 (1982).

[11] C.B. Chitwood *et al.*, Phys. Lett. B **131**, 289 (1983).

[12] A. Bujak *et al.*, Phys. Rev. C **32**, 620 (1985).

[13] W.G. Lynch, Ann. Rev. Nucl. Part. Sci. **37**, 493 (1987).

[14] M. E. Fischer, Rep. Prog. Phys. **67**, 615 (1967).

[15] M. L. Gilkes *et al.*, Phys. Rev. Lett. **73**, 1590 (1994).

[16] S. Albergo *et al.*, Nuovo Cimento A **89**, 1 (1985).

[17] J. Natowitz *et al.*, Phys. Rev. C **52**, R2322 (1995).

[18] M.B. Tsang *et al.*, Phys. Rev. C **53**, R1057 (1996).

[19] X. Campi, H. Krivine and E. Plagnol, Phys. Lett. B **385** 1, (1996).

[20] L.G. Moretto *et al.*, Phys. Rev. Lett. **76**, 2822 (1996).

[21] L. Phair *et al.*, Phys. Rev. Lett. **75**, 213 (1995).

[22] L.G. Moretto *et al.*, Phys. Rev. Lett. **76**, 372 (1996).

[23] L.G. Moretto *et al.*, Phys. Rev. Lett. **74**, 1530 (1995).

[24] J.A. Lopez and J. Randrup, Nucl. Phys. A **503**, 183 (1989).

[25] J.A. Lopez and J. Randrup, Nucl. Phys. A **512**, 345 (1990).

[26] L.G. Moretto *et al.*, Phys. Rep. **287**, 249 (1997).

[27] R. Ghetti *et al.*, to be published, LBL-39196.

[28] W. Bauer, Phys. Rev. **C38**, 1297 (1988).

Ernest Orlando Lawrence Berkeley National Laboratory
One Cyclotron Road | Berkeley, California 94720

Prepared for the U.S. Department of Energy under Contract No. DE-AC03-76SF00098